NANO LETTERS

Letter

pubs.acs.org/NanoLett

Measuring Lattice Strain in Three Dimensions through Electron Microscopy

Bart Goris,[†] Jan De Beenhouwer,[‡] Annick De Backer,[†] Daniele Zanaga,[†] K. Joost Batenburg,[§] Ana Sánchez-Iglesias,[⊥] Luis M. Liz-Marzán,[⊥,¶] Sandra Van Aert,[†] Sara Bals,*[,†] Jan Sijbers,[‡] and Gustaaf Van Tendeloo[†]

[†]Electron Microscopy for Materials Research (EMAT), University of Antwerp, Groenenborgerlaan 171, 2020 Antwerp, Belgium

[‡]iMinds-Vision Lab, University of Antwerp, Universiteitsplein 1, 2610 Wilrijk, Belgium

[§]Centrum Wiskunde & Informatica, P.O. Box 94079, 1090 GB Amsterdam, The Netherlands

[⊥]Bionanoplasmonics Laboratory, CIC biomaGUNE, Paseo de Miramón 182, 20009 Donostia - San Sebastian, Spain

[¶]Ikerbasque, Basque Foundation for Science, 48013 Bilbao, Spain

Supporting Information

ABSTRACT: The three-dimensional (3D) atomic structure of nanomaterials, including strain, is crucial to understand their properties. Here, we investigate lattice strain in Au nanodecahedra using electron tomography. Although different electron tomography techniques enabled 3D characterizations of nanostructures at the atomic level, a reliable determination of lattice strain is not straightforward. We therefore propose a novel model-based approach from which atomic coordinates are measured. Our findings demonstrate the importance of investigating lattice strain in 3D.

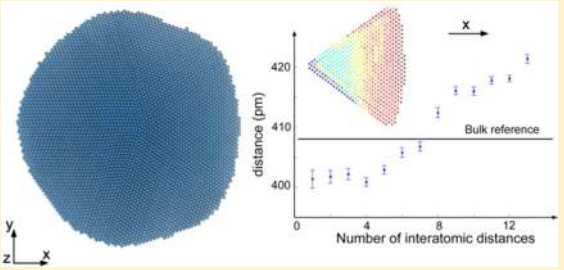

KEYWORDS: *Atomic resolution, electron tomography, Au nanodecahedron, 3D lattice strain*

The structural characterization of nanoparticles is an important topic in materials science since many properties heavily depend on size and morphology. The crystal structure, including defects and (surface) strain, is just as essential since it will directly affect plasmonic or catalytic properties.[1−3] To fully understand the connection between the presence of lattice strain and the properties of nanoparticles, it is crucial to measure the strain in a reliable manner. The distribution of strain in nanocrystals is usually investigated using coherent X-ray diffraction techniques and using a combination of pair distribution function and extended X-ray absorption fine structure (EXAFS).[4−6] On a more local scale, transmission electron microscopy (TEM) techniques, such as electron holography and electron diffraction, have been applied.[7−13]

A very challenging example of strained nanoparticles consists of the so-called "nanodecahedra" or "pentagonal bipyramids". Such particles consist of five segments bound by {111} twin boundaries, yielding a crystallographically forbidden morphology. Indeed, the angle between the crystallographic <111> directions equals 70.53°, resulting in an overall missing gap of 7.35°. To fill this gap, the atomic arrangement in each segment must contain significant displacements, resulting in large intrinsic strain fields. Among the models that have been proposed to explain the internal structure of nanodecahedrons, two of them are most accepted. The homogeneous strain model suggests that the structure consists of five segments that change from face-centered cubic (fcc) to a body-centered orthorhombic (bco) structure.[14,15] The inhomogeneous strain model includes a central defect, corresponding to a so-called single wedge disclination that coincides with the five-fold axis of the nanoparticle. This produces an inhomogeneous strain field that reduces the total strain energy.[16,17]

Measuring strain fields in nanodecahedra using TEM has been the topic of several studies during recent years. Hÿtch and co-workers combined atomic resolution TEM and geometrical phase analysis (GPA) to investigate the strain distribution in a Au decahedron with a diameter of 17 nm.[10] Their results, supported by finite element calculations, revealed a combination of an internal lattice rotation and small shear strains inside each segment of the nanoparticle. By using a quantitative statistical analysis, displacement maps based on aberration corrected TEM images of Au nanodecahedrons with a size of 5 nm were obtained by Walsh and co-workers.[18] In this manner, an average expansion of the lattice parameters of 5.6% at the surface of Au decahedrons was determined. Although these studies provide a good start toward the understanding of the strain distribution inside Au decahedrons, it is important to note that the results are based on a single two-dimensional (2D) projection, hereby neglecting the three-dimensional (3D) nature of the lattice strain. We therefore aimed at comparing

Received: July 30, 2015
Revised: August 28, 2015

DOI: 10.1021/acs.nanolett.5b03008
Nano Lett. XXXX, XXX, XXX−XXX

such 2D strain investigations with 3D measurements based on high-resolution electron tomography reconstructions.

Electron tomography is a technique that yields a 3D reconstruction of an object based on a series of 2D projection images acquired at different tilt angles.[19,20] Recently, different methods have been proposed to push the 3D spatial resolution to the atomic scale.[21−23] Discrete tomography in combination with atom counting enabled a high resolution 3D characterization of nanostructures, but since the atom positions were fixed during the reconstruction, displacement fields could not be calculated.[23,24] Scott et al. reported the reconstruction of an icosahedral Au nanoparticle with a resolution up to 2.4 Å based on an equally sloped tomography algorithm, but not all atom positions could be recovered.[22,25] Surface relaxation in a defect-free Au nanorod was studied using atomic resolution electron tomography based on compressive sensing.[21,26] This approach uses a limited number of high resolution projection images that should be acquired along specific zone axes of the sample. For Au nanodecahedrons, the number of suitable axes that can be reached, even using a dedicated tomography holder, is restricted to only one.

Although all of these studies prove the feasibility of atomic resolution electron tomography, a dedicated analysis of the final reconstructions is required to measure lattice strain.[21,27] In addition to many technical challenges during the acquisition and the reconstruction, one of the main problems is that 3D reconstructions at the atomic scale often correspond to a continuous tensor of intensity values hampering the extraction of the exact coordinates of the atoms inside the nanoparticle. To overcome these limitations, we propose a novel reconstruction algorithm in which each atom is modeled by a 3D Gaussian function. This enables a direct calculation of the coordinates of every atom in the nanoparticle from which the strain distribution can be extracted in a straightforward manner.

Au nanodecahedrons were prepared by silver-assisted seeded growth in the presence of benzyldimethylhexadecylammonium chloride (BDAC). Figure 1, panel a displays a high-resolution high-angle annular dark field (HAADF) scanning transmission electron microscopy (STEM) image of a Au decahedron acquired along the [110] zone-axis. From this projection image, the five-folded symmetry is obvious. Furthermore, as indicated by white arrows in Figure 1, panel a, additional planar defects in two out of five segments can be observed. It is known that such additional defects are commonly generated in decahedrons to relieve the large elastic strain energy.[28] To determine the positions of the atomic columns from Figure 1, panel a, we applied statistical parameter estimation theory, a technique that allows us to fit a set of Gaussian peaks to atomic resolution (S)TEM images, yielding estimations for the 2D coordinates of each atomic column. In this manner, a 2D displacement map with respect to a reference region can be extracted.[29−32] For this particle, the reference region is the center of a segment. By calculating derivatives of the displacement map, the strain distribution in the particle was investigated, similar to the approach used by Galindo and co-workers.[33] The resulting ε_{xx} component for one of the segments is presented in Figure 1, panel b, and no significant strain or lattice variations are observed. The ε_{yy} map is of less interest when investigating surface relaxation and was therefore not further analyzed in this context.

On the basis of the estimations for the 2D coordinates of each atomic column, the variation of the lattice parameters along x was investigated for the area indicated by a white

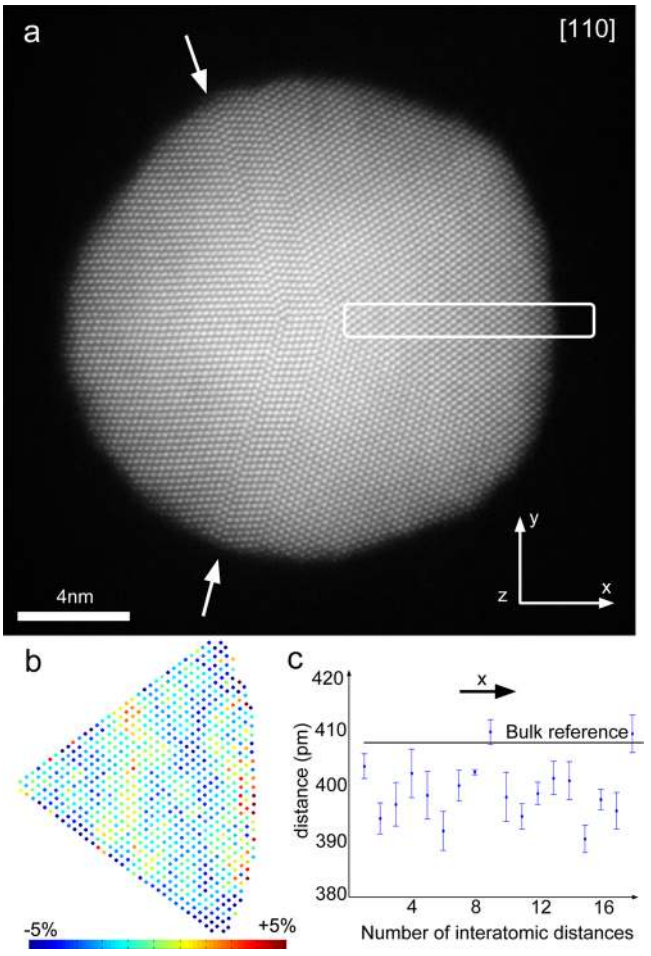

Figure 1. 2D analysis of strain distribution based on a HAADF-STEM projection image. (a) HAADF-STEM projection image of a Au nanodecahedron oriented along its [110] zone axis so that all five segments constituting the entire nanoparticle are visible. As indicated by the white arrows, additional defects were found in two out of five segments. (b) ε_{xx} strain map of one selected segment of the Au decahedron. The strain distribution is visualized using a color code and scaled between ±5%. (c) Variation of the lattice parameter along x, measured for the region indicated by a white rectangle in panel a. Both panels b and c do not indicate significant strain.

rectangle in Figure 1, panel a. The mean interatomic distances and corresponding standard deviations are calculated from sets of equivalent distances. The pixel size for this figure (24.7 pm) was calibrated using a standard Au thin film used during the TEM alignment for which we assume that the lattice parameter of Au equals 0.408 nm. From Figure 1, panel c, it is again clear that no systematic variation of the lattice parameter is observed. It must be noted, however, that based on Figure 1, only displacements of the atoms averaged along the z-direction are measured. Next, we will compare these 2D results with a 3D analysis based on an atomic scale 3D reconstruction of the same Au nanodecahedron.

A tilt series of 2D projection images was acquired using an aberration corrected FEI Titan^3 microscope in HAADF-STEM mode over a tilt range of −74° to +68° with a 2° tilt increment. The alignment of the tilt series is always critical to obtain high quality 3D reconstructions. During a conventional alignment, the angles at which the images in the tilt series are acquired are fixed according to their nominal values. Here, the angles were estimated during the reconstruction in an iterative manner by

DOI: 10.1021/acs.nanolett.5b03008
Nano Lett. XXXX, XXX, XXX−XXX

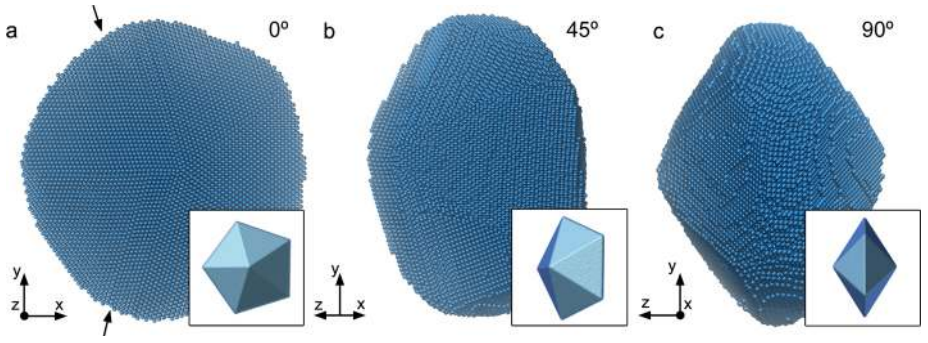

Figure 2. 3D visualization of a reconstructed nanoparticle. (a–c) 3D visualizations of the tomographic reconstruction of a Au nanodecahedron containing more than 90 000 atoms, oriented along three different directions that are rotated over 0°, 45°, and 90°, respectively. The arrows in panel a indicate planar defects inside the decahedron.

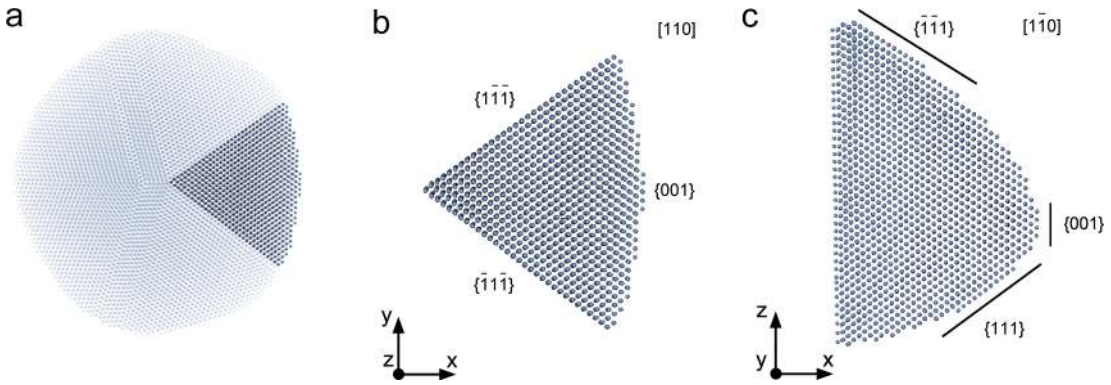

Figure 3. Detailed analysis of the surface morphology of a reconstructed segment. (a) Overview of the 3D reconstruction indicating the investigated segment. (b) Magnified visualization of the segment oriented along a [110] zone axis. (c) The same region, viewed along a [1−10] zone axis, which is orthogonal to the viewing direction presented in panel b. These visualizations indicate that the morphology of each segment is mainly composed of {111} facets.

calculating intermediate reconstructions. The alignment parameters are hereby optimized such that the projection distance between original projection images and forward projected images from an intermediate reconstruction is minimized.[34] Technical details on this approach are provided in the Methods section.

As discussed earlier, the outcome of a 3D reconstruction at the atomic scale is often a continuous 3D volume of intensity values, from which the center of each atom can only be determined by additional analysis after the reconstruction. Very often it is therefore impossible to obtain atom coordinates because of the size of the data set and the lack of objective and automatic segmentation procedures. Here, we overcome this limitation by assuming that the 3D atomic potential can be modeled by 3D Gaussian functions. Although this is a moderate hypothesis, it significantly simplifies the reconstruction problem to a sparse inverse problem, yielding the coordinates of the individual atoms as a direct outcome of the reconstruction. Although the method can be extended to a more general object that better reflects the behavior of the atomic electron density in the vicinity of the nucleus, such as a sum of Gaussians or a Lorentzian, this is only possible at the expense of computational costs. Therefore, a continuous reconstruction algorithm is alternated with a peak finding method that extracts the positions at which Gaussian functions are most likely located. Remarkably, no prior knowledge concerning the crystal structure is assumed during the reconstruction. Additional details on the reconstruction technique can be found in the Methods section.

Visualizations of the final 3D reconstruction obtained for the Au nanodecahedron, containing more than 90 000 atoms, are presented in Figure 2 along different viewing directions. The inset displays the 3D model of the morphology, and an animated view is provided in the Supporting Information.

To verify the crystal structure of the reconstructed decahedron, the atomic coordinates were studied by the method of Steinhardt bond order parameters, which provides information about the symmetry of the bond orientations.[35,36] Bonds are defined as the vectors that interconnect two neighboring atoms. The result is provided in the Supporting Information and is consistent with an fcc atomic arrangement. This is in contrast to the homogeneous strain model in which a transition from fcc to bco was proposed.

More detailed 3D visualizations of a single segment along different [110] zone axes are presented in Figure 3, panels b and c, which demonstrate that the top and bottom surfaces of the segment are mainly composed of {111} facets with small additional {001} facets at the edge of the nanoparticle. The presence of large {111} facets is in agreement with previous studies in which the morphology was investigated by thickness profiles and electron tomography at the nanometer scale.[37,38] Moreover, the presence of {111} facets was expected based on thermodynamic equilibrium since the relations between the surface energies of the low-index facets are given by $\gamma_{\{111\}} < \gamma_{\{001\}} < \gamma_{\{110\}}$.[39−41]

One of the most important advantages of our approach is that the reconstruction yields all atom coordinates as a direct output. In this manner, it becomes straightforward to calculate

DOI: 10.1021/acs.nanolett.5b03008
Nano Lett. XXXX, XXX, XXX−XXX

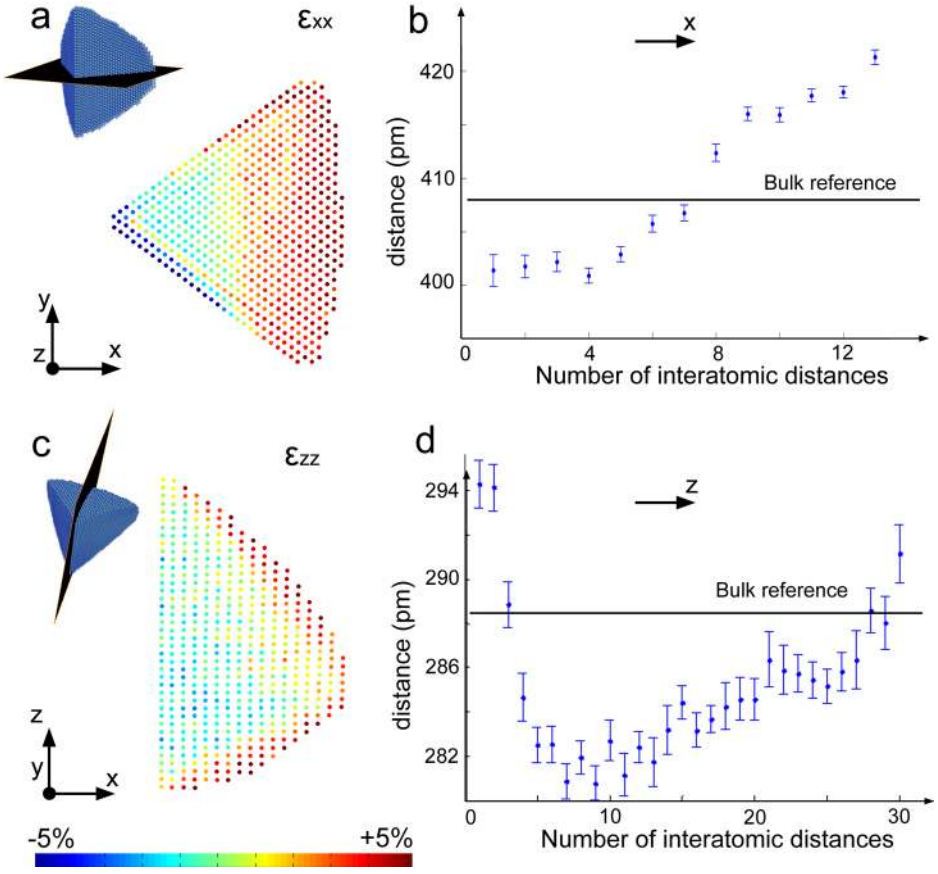

Figure 4. 3D strain analysis. (a) Slice through the ε_{xx} volume. The strain distribution is visualized using a color code and scaled between ±5%. (b) Variation of the lattice parameter along x. The mean interatomic distances and corresponding standard deviations are calculated from sets of equivalent distances in consecutive slices. (c) Slice through the ε_{zz} volume. The strain distribution is visualized using a color code and scaled between ±5%. (d) Variation of the lattice parameter along z. The mean interatomic distances and corresponding standard deviations are calculated from sets of equivalent distances in consecutive slices.

the 3D displacement map. Again the displacements were calculated with respect to a reference region in the middle of the segment displayed in Figure 1. We computed derivatives of the displacement map in such a manner that 3D volumes are obtained corresponding to ε_{xx} and ε_{zz}. Slices through the resulting ε_{xx} and ε_{zz} volumes were acquired through the middle of the segment, and the results are presented in Figure 4, panels a and c. Furthermore, the variation of the lattice parameters was investigated along x and z based on the same slices (Figure 4, panels b and d). Both along the x and z direction, a systematic outward expansion of the lattice can be observed. The expansion along z is limited to a few of the outer atomic layers and shows an asymmetry (Figure 4, panel d) that is likely to be related to the fact that the decahedron is deposited on a carbon support.

The first important finding is the fact that our 3D results enable us to determine an outward lattice expansion of the particle along the z direction. It should be stressed that this is only possible through a 3D approach such as the one presented here since displacements along the z direction cannot be extracted from a single projection image. For the nanoparticle under investigation, a relative expansion of approximately 5% is observed, which can be expected to have a significant influence on the physical properties. Although the value that we extract from our 3D results is comparable to the 2D results by Walsh et al.,[18] a direct comparison is not straightforward since the particle investigated in this study is approximately five times larger.

Furthermore, the 2D projection image in Figure 1 suggested negligible displacements in the x direction, whereas the analysis in Figure 4, panels a and b, suggested a systematic outward expansion. This can be understood since Figure 1 only provides average information. In Supporting Figure 2, we show that slices acquired at different positions through the 3D reconstruction show different ε_{xx} strain distributions. The observed asymmetry is probably again related to the fact that the decahedron is deposited on a carbon support. As a consequence of the averaging along z, no systematic displacements along the x direction are obtained in a projection image. This is confirmed by Supporting Figure 3, where the forward projection of the 3D reconstruction is presented. This forward projection was analyzed in a similar manner as Figure 1. The excellent agreement between Figure 1 and Supporting Figure 3 proves the reliability of the 3D reconstruction and once more demonstrates the importance of measuring the lattice strain from a 3D reconstruction. Also, the expansion along the z direction was investigated for different slices through the 3D reconstruction (Supporting Figure 4). Here, we conclude that the outer expansion is always present and limited to a few of the outer atomic layers.

In conclusion, we present a novel technique to obtain 3D reconstructions at the atomic scale using a model-based approach from which atomic coordinates can be extracted in

DOI: 10.1021/acs.nanolett.5b03008
Nano Lett. XXXX, XXX, XXX−XXX

a straightforward manner. This methodology enabled us to investigate a Au nanodecahedron consisting of more than 90 000 atoms. A careful investigation of the lattice strain was carried out in 3D and compared to the 2D results. The use of 2D projection images only was found to lead to an incomplete characterization since the 3D reconstruction indicates significant displacements of the atoms along the z direction. Our findings suggest the importance of investigating displacement fields from 3D reconstructions. The methodology is applied here to a Au nanodecahedron, but the technique is applicable to a broad range of nanostructures. The 3D atomic scale information that can be obtained using our approach will highly contribute to a complete understanding of the physical behavior of nanomaterials.

■ ASSOCIATED CONTENT

Supporting Information

The Supporting Information is available free of charge on the ACS Publications website at DOI: 10.1021/acs.nanolett.5b03008.

Methods section; visualizations of the ε_{xx} and ε_{zz} strain fields obtained at different positions in the reconstruction; strain field obtained from the forward projection; analysis of the reconstruction based on Steinhardt bond order parameter method (PDF)

Animated view of the 3D reconstruction (AVI)

■ AUTHOR INFORMATION

Corresponding Author

*E-mail: sara.bals@uantwerpen.be.

Author Contributions

B.G. and J.D.B. contributed equally to this work.

Notes

The authors declare no competing financial interest.

■ ACKNOWLEDGMENTS

The work was supported by the Research Foundation Flanders (FWO Vlaanderen) and by research grants to B.G. and A.D.B. S.B., D.Z., and L.M.L.-M. acknowledge funding from the European Research Council (Starting Grant No. COLOURATOMS 335078, Advanced Grant No. PLASMAQUO 267867). The research leading to these results has received funding from the European Union Seventh Framework Programme under Grant Agreement Nos. 312483 (ESTEEM2) and 262348 (ESMI). K.J.B. acknowledges support by The Netherlands Organization for Scientific Research (NWO), Program No. 639.072.005.

■ REFERENCES

(1) Goubet, N.; Yan, C.; Polli, D.; Portales, H.; Arfaoui, I.; Cerullo, G.; Pileni, M. P. Modulating Physical Properties of Isolated and Self-Assembled Nanocrystals through Change in Nanocrystallinity. *Nano Lett.* **2013**, *13*, 504−508.

(2) Louis, C.; Pluchery, O. *Gold Nanoparticles for Physics, Chemistry, and Biology*; Imperial College Press: London, 2012.

(3) Novo, C.; Funston, A. M.; Mulvaney, P. Direct Observation of Chemical Reactions on Single Gold Nanocrystals Using Surface Plasmon Spectroscopy. *Nat. Nanotechnol.* **2008**, *3*, 598−602.

(4) Gilbert, B.; Huang, F.; Zhang, H. Z.; Waychunas, G. A.; Banfield, J. F. Nanoparticles: Strained and Stiff. *Science* **2004**, *305*, 651−654.

(5) Pfeifer, M. A.; Williams, G. J.; Vartanyants, I. A.; Harder, R.; Robinson, I. K. Three-Dimensional Mapping of a Deformation Field inside a Nanocrystal. *Nature* **2006**, *442*, 63−66.

(6) Ulvestad, A.; Clark, J. N.; Harder, R.; Robinson, I. K.; Shpyrko, O. G. 3D Imaging of Twin Domain Defects in Gold Nanoparticles. *Nano Lett.* **2015**, *15*, 4066−4070.

(7) Huang, W. J.; Sun, R.; Tao, J.; Menard, L. D.; Nuzzo, R. G.; Zuo, J. M. Coordination-Dependent Surface Atomic Contraction in Nanocrystals Revealed by Coherent Diffraction. *Nat. Mater.* **2008**, *7*, 308−313.

(8) Hytch, M.; Houdellier, F.; Hue, F.; Snoeck, E. Nanoscale Holographic Interferometry for Strain Measurements in Electronic Devices. *Nature* **2008**, *453*, 1086−1089.

(9) Hytch, M. J.; Snoeck, E.; Kilaas, R. Quantitative Measurement of Displacement and Strain Fields from HREM Micrographs. *Ultramicroscopy* **1998**, *74*, 131−146.

(10) Johnson, C. L.; Snoeck, E.; Ezcurdia, M.; Rodriguez-Gonzalez, B.; Pastoriza-Santos, I.; Liz-Marzan, L. M.; Hytch, M. J. Effects of Elastic Anisotropy on Strain Distributions in Decahedral Gold Nanoparticles. *Nat. Mater.* **2008**, *7*, 120−124.

(11) Newton, M. C.; Leake, S. J.; Harder, R.; Robinson, I. K. Three-Dimensional Imaging of Strain in a Single ZnO Nanorod. *Nat. Mater.* **2010**, *9*, 120−124.

(12) Randle, V.; Barker, I.; Ralph, B. Measurement of Lattice-Parameter and Strain Using Convergent Beam Electron-Diffraction. *J. Electron Microsc. Tech.* **1989**, *13*, 51−65.

(13) Wang, J.; Sansoz, F.; Deng, C.; Xu, G.; Han, G.; Mao, S. X. Strong Hall-Petch Type Behavior in the Elastic Strain Limit of Nanotwinned Gold Nanowires. *Nano Lett.* **2015**, *15*, 3865−3870.

(14) Bagley, B. G. A Dense Packing of Hard Spheres with 5-Fold Symmetry. *Nature* **1965**, *208*, 674−675.

(15) Yang, C. Y. Crystallography of Decahedral and Icosahedral Particles 0.1. Geometry of Twinning. *J. Cryst. Growth* **1979**, *47*, 274−282.

(16) de Wit, R. Partial Disclinations. *J. Phys. C: Solid State Phys.* **1972**, *5*, 529−534.

(17) Marks, L. D.; Howie, A. Multiply-Twinned Particles in Silver Catalysts. *Nature* **1979**, *282*, 196−198.

(18) Walsh, M. J.; Yoshida, K.; Kuwabara, A.; Pay, M. L.; Gai, P. L.; Boyes, E. D. On the Structural Origin of the Catalytic Properties of Inherently Strained Ultrasmall Decahedral Gold Nanoparticles. *Nano Lett.* **2012**, *12*, 2027−2031.

(19) Midgley, P. A.; Dunin-Borkowski, R. E. Electron Tomography and Holography in Materials Science. *Nat. Mater.* **2009**, *8*, 271−280.

(20) Midgley, P. A.; Weyland, M. 3D Electron Microscopy in the Physical Sciences: The Development of Z-Contrast and EFTEM Tomography. *Ultramicroscopy* **2003**, *96*, 413−431.

(21) Goris, B.; Bals, S.; Van den Broek, W.; Carbo-Argibay, E.; Gomez-Grana, S.; Liz-Marzan, L. M.; Van Tendeloo, G. Atomic-Scale Determination of Surface Facets in Gold Nanorods. *Nat. Mater.* **2012**, *11*, 930−935.

(22) Scott, M. C.; Chen, C. C.; Mecklenburg, M.; Zhu, C.; Xu, R.; Ercius, P.; Dahmen, U.; Regan, B. C.; Miao, J. W. Electron Tomography at 2.4-Angstrom Resolution. *Nature* **2012**, *483*, 444−447.

(23) Van Aert, S.; Batenburg, K. J.; Rossell, M. D.; Erni, R.; Van Tendeloo, G. Three-Dimensional Atomic Imaging of Crystalline Nanoparticles. *Nature* **2011**, *470*, 374−377.

(24) Bals, S.; Casavola, M.; van Huis, M. A.; Van Aert, S.; Batenburg, K. J.; Van Tendeloo, G.; Vanmaekelbergh, D. Three-Dimensional Atomic Imaging of Colloidal Core-Shell Nanocrystals. *Nano Lett.* **2011**, *11*, 3420−3424.

(25) Chen, C. C.; Zhu, C.; White, E. R.; Chiu, C. Y.; Scott, M. C.; Regan, B. C.; Marks, L. D.; Huang, Y.; Miao, J. W. Three-Dimensional Imaging of Dislocations in a Nanoparticle at Atomic Resolution. *Nature* **2013**, *496*, 74−77.

(26) Goris, B.; De Backer, A.; Van Aert, S.; Gomez-Grana, S.; Liz-Marzan, L. M.; Van Tendeloo, G.; Bals, S. Three-Dimensional Elemental Mapping at the Atomic Scale in Bimetallic Nanocrystals. *Nano Lett.* **2013**, *13*, 4236−4241.

(27) Xu, R.; Chen, C.-C.; Wu, L.; Scott, M. C.; Theis, W.; Ophus, C.; Bartels, M.; Yang, Y.; Ramezani-Dakhel, H.; Sawaya, M. R.; Heinz, H.; Marks, L. D.; Ercius, P.; Miao, J. Three-dimensional coordinates of

DOI: 10.1021/acs.nanolett.5b03008
Nano Lett. XXXX, XXX, XXX−XXX

individual atoms in materials revealed by electron tomography. *ArXiv:1505.05938*. **2015**.
(28) Zhou, Y.; Fichthorn, K. A. Internal Stress-Induced Orthorhombic Phase in 5-Fold-Twinned Noble Metal Nanowires. *J. Phys. Chem. C* **2014**, *118*, 18746−18755.
(29) Bals, S.; Van Aert, S.; Van Tendeloo, G.; Avila-Brande, D. Statistical Estimation of Atomic Positions from Exit Wave Reconstruction with a Precision in the Picometer Range. *Phys. Rev. Lett.* **2006**, *96*.10.1103/PhysRevLett.96.096106
(30) den Dekker, A. J.; Gonnissen, J.; De Backer, A.; Sijbers, J.; Van Aert, S. Estimation of Unknown Structure Parameters from High-Resolution (S)TEM Images: What Are the Limits? *Ultramicroscopy* **2013**, *134*, 34−43.
(31) Van Aert, S.; Turner, S.; Delville, R.; Schryvers, D.; Van Tendeloo, G.; Salje, E. K. H. Direct Observation of Ferrielectricity at Ferroelastic Domain Boundaries in $CaTiO_3$ by Electron Microscopy. *Adv. Mater.* **2012**, *24*, 523−527.
(32) Van Aert, S.; Van den Broek, W.; Goos, P.; Van Dyck, D. Model-Based Electron Microscopy: From Images toward Precise Numbers for Unknown Structure Parameters. *Micron* **2012**, *43*, 509−515.
(33) Galindo, P. L.; Kret, S.; Sanchez, A. M.; Laval, J. Y.; Yanez, A.; Pizarro, J.; Guerrero, E.; Ben, T.; Molina, S. I. The Peak Pairs Algorithm for Strain Mapping from HRTEM Images. *Ultramicroscopy* **2007**, *107*, 1186−1193.
(34) De Beenhouwer, J.; Sijbers, J. In *Markerless 3D Alignment of an Electron Tomogram*. The 7th International Electron Tomography Conference, Cancun, Mexico, 2014.
(35) Steinhardt, P. J.; Nelson, D. R.; Ronchetti, M. Bond-Orientational Order in Liquids and Glasses. *Phys. Rev. B: Condens. Matter Mater. Phys.* **1983**, *28*, 784−805.
(36) Wang, Y. T.; Teitel, S.; Dellago, C. Melting of Icosahedral Gold Nanoclusters from Molecular Dynamics Simulations. *J. Chem. Phys.* **2005**, *122*, 214722.
(37) Batenburg, K. J.; Bals, S.; Sijbers, J.; Kubel, C.; Midgley, P. A.; Hernandez, J. C.; Kaiser, U.; Encina, E. R.; Coronado, E. A.; Van Tendeloo, G. 3d Imaging of Nanomaterials by Discrete Tomography. *Ultramicroscopy* **2009**, *109*, 730−740.
(38) Cantu-Valle, J.; Ruiz-Zepeda, F.; Voelkl, E.; Kawasaki, M.; Santiago, U.; Jose-Yacaman, M.; Ponce, A. Determination of the Surface Morphology of Gold-Decahedra Nanoparticles Using an Off-Axis Electron Holography Dual-Lens Imaging System. *Micron* **2013**, *54*−*55*, 82−86.
(39) Liu, T. J.; Jiang, P.; You, Q.; Ye, S. F. Five-Fold Twinned Pentagonal Gold Nanocrystal Structure Exclusively Bounded by {110} Facets. *CrystEngComm* **2013**, *15*, 2350−2353.
(40) Patala, S.; Marks, L. D.; de la Cruz, M. O. Thermodynamic Analysis of Multiply Twinned Particles: Surface Stress Effects. *J. Phys. Chem. Lett.* **2013**, *4*, 3089−3094.
(41) Patala, S.; Marks, L. D.; de la Cruz, M. O. Elastic Strain Energy Effects in Faceted Decahedral Nanoparticles. *J. Phys. Chem. C* **2013**, *117*, 1485−1494.

DOI: 10.1021/acs.nanolett.5b03008
Nano Lett. XXXX, XXX, XXX−XXX